2020 NDIA GROUND VEHICLE SYSTEMS ENGINEERING AND TECHNOLOGY SYMPOSIUM
MODELING SIMULATION & SOFTWARE TECHNICAL SESSION
AUGUST 11-13, 2020 - NOVI, MICHIGAN

REMOTE SENSING OF TERRAIN STRENGTH FOR MOBILITY MODELING & SIMULATION

Jordan Ewing[1], Thomas Oommen, PhD[1], Paramsothy Jayakumar, PhD[2], Russell Alger[3]

[1]Geological Mining and Engineering Department, Michigan Technological University, Houghton, MI
[2]Analytics, US ARMY CCDC Ground Vehicle Systems Center, Warren, MI
[3]Keweenaw Research Center, Houghton, MI

ABSTRACT

Knowing the soil's strength properties is a vital component to accurately develop Go/No-Go mobility maps for the Next Generation NATO Reference Mobility Model (NG-NRMM). The Unified Soil Classification System (USCS) and soil strength of the top 0-6" and 6-12" of the soil are essential terrain inputs for the model. Current methods for the NG-NRMM require in-situ measurement of soil strength using a bevameter, cone penetrometer, or other mechanical contact device. This study examines the use of hyperspectral and thermal imagery to provide ways of remotely characterizing soil type and strength. Hyperspectral imaging provides unique spectrums for each soil where a Soil Classification Index (SCI) was developed to predict the gradation of the soil types. This gradation provides a means of identifying the soil type via the major divisions within the USCS classification system. Thermal imagery is utilized to collect the Apparent Thermal Inertia (ATI) for each pit, which is then correlated to the soil strength.

Citation: J. Ewing, T. Oommen, P. Jayakumar, R. Alger, "Remote Sensing of Terrain Strength for Mobility Modeling Simulation & Software", In *Proceedings of the Ground Vehicle Systems Engineering and Technology Symposium* (GVSETS), NDIA, Novi, MI, Aug. 11-13, 2020.

1. INTRODUCTION

There is work currently being done to characterize terrain strength and land mapping for autonomous mobility and simulation modeling. The mobility of military vehicles in unknown territories is one such example. The terrain strength parameter is one of the critical inputs for developing the Go/No-Go mobility maps that are used for autonomous mobility. Past models for characterizing the terrain strength have relied primarily on in-situ measurements. Bevameters have been the traditional best choice for the in-situ approximation of soil strength [1]. The bevameter is quite expensive and difficult to transport, so the cone penetrometer is an excellent second choice for collecting terrain strength [1, 2]. However, in-situ measurements are challenging to obtain in war-

zones and could potentially place soldiers at risk. Therefore, developing alternate approaches for in-situ terrain strength characterization is a priority for autonomous mobility [3].

Another critical component for the mobility maps is knowing the soil type of the area. The standard for characterizing a soil type within engineering is the Unified Soil Classification System (USCS), which describes the gradation and texture of a soil [4]. Having a standardized soil classification via the USCS is useful to help develop soil type mapping. One of the essential details that control the physical and mechanical properties of the soil is the grain size distribution (gradation). The gradation of a soil carries key details about the soil's mechanical behavior, studies have shown that one could create an index to correlate to these values [5].

An alternative for in-situ soil characterization is the use of remote sensing technology. Remote sensing has evolved with more computational capabilities and improved sensors to be a more time-efficient and accurate tool that continues to grow [6]. Remote sensing offers an efficient and rapid collection over an area of interest safely and cost-effectively. Stark [7] has done previous work studying the use of cameras, Unmanned Aerial Vehicles (UAV)s, and satellites to estimate sand lower bound friction angles and bearing strength. Remote sensing has many different types, based on the wavelength used for sensing and spectral resolution such as hyperspectral, multispectral, thermal, etc.

Hyperspectral imaging is one branch of remote sensing that has been used for the improvement of target recognition, and background characterization [8], show potential to provide new methods for soil mapping [9], and can be used to estimate different features for a bare soil [10]. Thermal remote sensing provides a simple approach to getting information about the subsurface properties of the soil. Archeologists have used this for identifying the location of buried structures [11] and buried objects [12]. It has also similarly been used to quantify moisture at soil sites and mine tailings [13], and relating Thermal Inertia (TI) / Apparent Thermal Inertia (ATI) to land use/land cover mapping [14]. ATI has been used for studying mobility purposes as well [15], identifying the morphology and composition of Mars [16], and TI for examining heterogeneity of Mars [17]

As a non-destructive and efficient data collection method, remote sensing shows great promise for soil characterization purposes. For our approach, we examine the use of hyperspectral remote sensing within the visible and near-infrared (NIR) range (400-1000nm). We show the use of hyperspectral imagery to provide a soil classification index, which in turn helps predict the gradation of five distinct soil types. In addition, using thermal imaging, we look at the utility of the ATI to predict the soil strength of each soil type in terms of soil stiffness and cone penetrometer measurements. We hypothesis that ATI being a function of the object property of the material, will be correlated to the strength of the soil. All leading to a safe, effective means for developing mobility maps without putting soldiers at risk.

2. METHODOLOGY

In this study, we used five different soil types from the mobility tracks at the Keweenaw Research Center (KRC). The soil type at these tracks is known as Fine, Coarse, Rink, Stability, and 2NS, which contain different amounts of gravel, sand, and fine particles. Figure 1 shows the original locations, and Table 1 lists the % gravel, % sand, and % fine content for each of the soil types.

Figure 1: Five soil locations on-site at the Keweenaw Research Center, Houghton, Michigan

Table 1: The % gravel, % sand, % fine content, and USCS classification for each of the soil types obtained from KRC.

	Fine	Coarse	Rink	Stability	2NS
% Gravel	0.0	16.8	10.7	31.1	0.6
% Sand	40.6	73.7	66.4	58.8	97.3
% Fine	59.4	9.5	23.0	10.0	2.1
USCS Classification	ML = Sandy Silt	SP-SM = Poorly Graded Sand with Silt and Gravel	SM = Silty Sand	SW-SM = Well Graded Sand with Silt and Gravel	SP = Poorly Graded Sand

2.1. Remote Sensing

Remote sensing is the process of quantifying the physical characteristics of an object by measuring the reflected and emitted components of the Electro-Magnetic (EM) spectrum. The variations in the characteristics of an object such as roughness, texture, colors, etc. influence the reflectance or emittance of the EM spectrum. This influence leads to unique spectral characteristics for different objects. Different cameras can detect the different wavelengths of the EM spectrum [18-20]. Some cameras can sense several narrow EM wavelengths, whereas some other cameras can detect fewer broader EM wavelengths. Depending on the number of wavelengths and the width of the wavelength that the camera can sense, it can be differentiated as a multispectral or hyperspectral camera. A multispectral camera typically detects few bands (e.g., 3 to 10 bands), with each band being a broader wavelength. On the other hand, the hyperspectral camera detects a large number of bands (e.g., hundreds or thousands of bands), with each band being a narrower wavelength. Remote sensing cameras are also classified based on the wavelength range that it measures.

In this study, we use a hyperspectral camera that is sensitive to the visible and near-infrared spectrum (400-1000 nm) that captures 120 bands with spectral accuracy of ~ 5-7 nm full width at half maximum (FWHM). We also use a thermal camera (7.5-13.5 μm) which quantifies the temperature of an object. Thermal imagery measures the emitted radiance of the material, quantifying the material's bulk properties. The thermal remote sensing provides a unique opportunity to understand the bulk properties of the object based on its emittance. In contrast, most other spectral wavelength measurements capture the reflected property from the surface of the object.

2.2. Thermal Inertia / Apparent Thermal Inertia

Thermal Inertia (TI) is a measure of the object to absorb and store heat in an object. Equation 1 displays the formula for estimating the TI of a material, where k is the thermal conductivity, ρ is the bulk density, and c is the specific heat [21, 22]. These parameters for TI require in-situ measurements. An approximation of the TI value, however, can be done via the Apparent Thermal Inertia (ATI) [22]. ATI can be remotely sensed by capturing two thermal images at different time points and estimating the albedo. Equation 2 gives the formula for calculating the ATI, where α is albedo and ΔT is the temperature difference.

$$TI = \sqrt{k\rho c} \quad (1)$$

$$ATI = (1 - \alpha)/\Delta T \quad (2)$$

2.3. Laboratory Testing

Laboratory experiments were carried out in a controlled environment. During these experiments each of the soils were separated into individual bins of 2ft x 2 ft x 1 ft (length x width x height) bins with two 500-Watt work lights one meter above each. The soils for each experiment were initially tested with a Humboldt GeoGauge (for soil stiffness) and volumetric water content (moisture) probes.

Following that a FLIR Duo R camera was used to collect the initial thermal image of the soil. Then the BaySpec hyperspectral camera was run along a track at nadir one meter above the soil surface. Finally at the end of 4 hours with heating from the work lights, the final thermal image was recorded for each pit.

2.4. Summer Field Work

In the summer of 2019, we expanded this study to the field and tested at the KRC test tracks where the soils used in the lab study were obtained. These soil pits are smoothed over by KRC, and various moisture contents for the soils were tested during the experiments. The field tests were carried out by mounting the BaySpec hyperspectral and FLIR thermal cameras to the UAV, where they were then flown on the UAV for collection, as seen in Figure 2.

Figure 2: UAV with loaded sensors (hyperspectral and thermal) (A), setup and calibration of the cameras (B), and UAV inflight to record over the Fine Pit (C).

After the morning flight, we went out and collected the GeoGauge stiffness value, ASD Handheld Pro (albedo), and cone penetrometer (cone index) for each pit. Multiple tests were done to collect each parameter in the middle and at each end of the pits. The moisture was collected each day via in-situ soil samples collected. A second thermal image required for estimating ATI was obtained using the UAV in the afternoon.

3. RESULTS

The laboratory experiments showed great promise for identifying unique reflectance spectrums for each soil from the hyperspectral imaging as shown in Figure 3. Utilizing these unique spectra, a Soil Classification Index (SCI) was developed. The SCI is computed based on three bands: 550 nm, 600 nm, and 650 nm (shown in Figure 3). The formula for calculating SCI is given by Equation 3, where R550 is the reflectance of the band at wavelength 550 nm, R600 and R650 similarly. This index has the ability to distinguish a soil's gradation, or rather, the % gravel, % sand, and % fine (whatever is remaining after % gravel and % sand) content of the soil. SCI works with four of the five soils for % gravel prediction (R^2 = 0.8291), and all soils for % sand (R^2 = 0.7496). The SCI's correlation between SCI to % gravel and % sand content is displayed in figure 4.

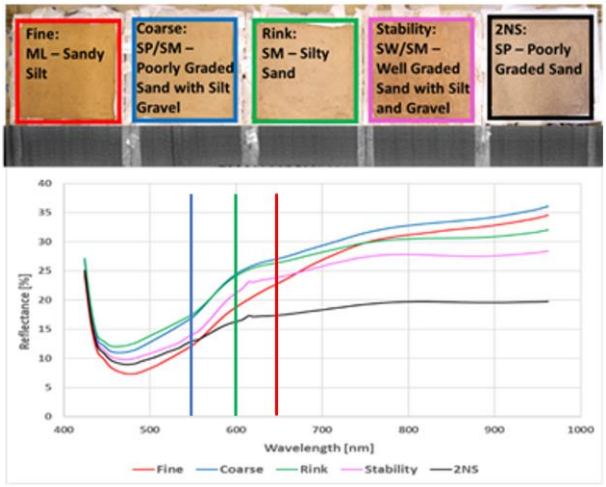

$$SCI = (R_{650} - R_{550})/R_{600} \quad (3)$$

Figure 3: Shows the hyperspectral plots for each soil and the location of the needed values for the soil classification index. Each colored box and the corresponding line are a different soil type. Going from left to right: Fine, Coarse, Rink, Stability, and 2NS. The range of the camera is from 400 – 1000 nm.

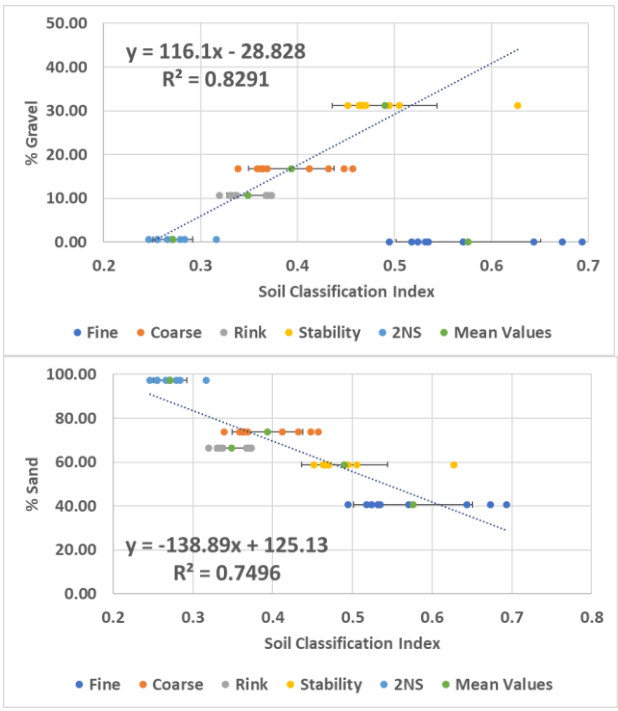

Figure 4: Trend lines for % gravel (top) and % sand (bottom) content among the five soils as recorded by the BaySpec hyperspectral camera.

Using SCI trends from the lab, prediction maps were built from the hyperspectral scans to identify soil gradation from the summer 2019 fieldwork at KRC. Examples of these prediction plots overlaid on the digital elevation models (DEMs) are shown in Figure 5. These soils then can be classified into their different gradations. Table 2 below shows what the actual and predicted gradation parameters of the soils are.

Figure 5: Examples of hyperspectral scans for gradation prediction maps for different soil pits overlaid on DEMs. 2NS pit % sand prediction plot (Left), Coarse pit (Right).

Table 2: Actual and Predicted values for the % gravel, % sand, % fine, D10, D30, D60, Cu, and Cc for each of the five soils.

SOILS (Actual /Predicted)	Fine (Act./Pred.)	Coarse (Act./Pred.)	Rink (Act./Pred.)	Stability (Act./Pred.)	2NS (Act./Pred.)
% Gravel	0.0 / 42.8	16.8 / 17.3	10.7 / 11.0	31.1 / 30.8	0.6 / 0.2
% Sand	40.6 / 41.2	73.7 / 71.0	66.4 / 78.4	58.8 / 55.3	97.3 / 91.0
% Fine	59.4 / 16.0	9.5 / 11.7	23.0 / 10.6	10.0 / 13.9	2.1 / 8.8

Next the remotely sensed ATI plots were overlaid onto the DEMs for each of the pits, as seen in Figure 6. Using the average ATI value from each soil pit, a linear relationship was found between the ATI and GeoGauge stiffness (Figure 7) for 4 of the five soil types. Another linear trend was also found for the ATI and cone penetrometer (Figure 8) strength values for all soil types, excluding Fine pit.

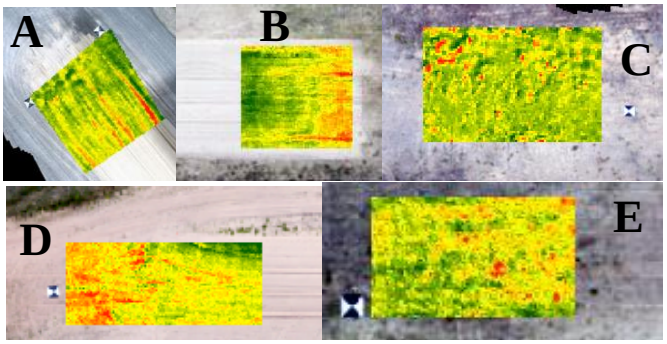

Figure 6: ATI prediction map for Fine pit overlaid on DEM. Green is low ATI and red is high ATI values. Fine (A), 2NS (B), Stability (C), Coarse (D), and Rink (E).

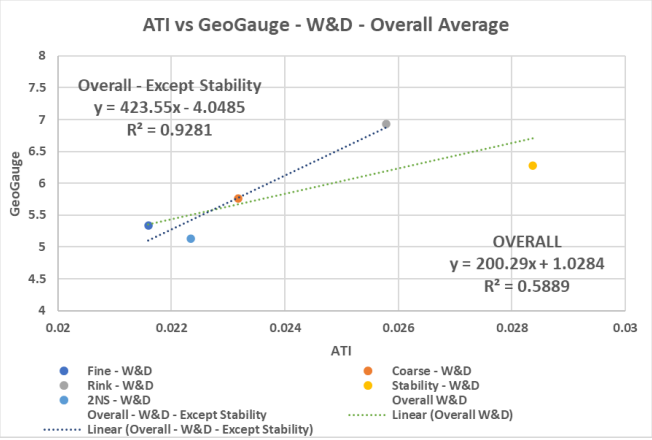

Figure 7: Relationship between Apparent Thermal Inertia (ATI) and GeoGauge stillness [Mega-Newton / meter].

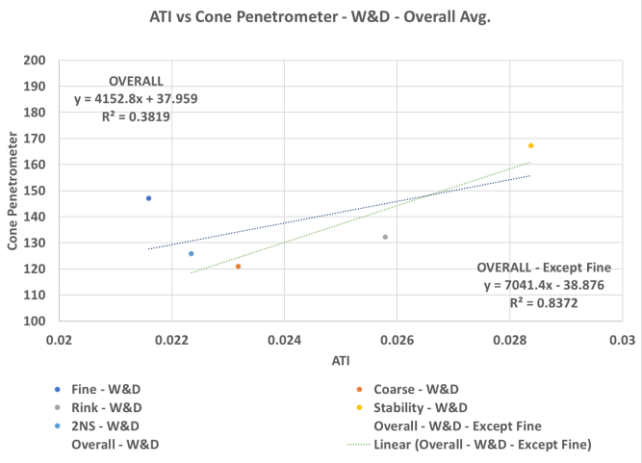

Figure 8: Relationship between Apparent Thermal Inertia (ATI) and cone penetrometer [psi].

4. ANALYSIS AND DISCUSSION

The SCI works for four of the five soil types examined for determining the % gravel content (R^2=0.8291) and works for all five soils for determining the % sand (R^2=0.7496). The only soil the SCI does not work for is the Fine soil pit. The SCI is delegated for gradation purposes, and when determining the % gravel, there is 0% gravel for the fine pit. Since there is no gravel versus even a little as is the case with 2NS, the Fine pit fails for predicting the % gravel. If further tests were developed to allow for more distinction within the "fine content" portion of the soil, one could then attempt to use the USCS system for classifying these pits.

Cone penetrometer was also able to be approximated for four of the five pits (not including Fine pit). It was also shown with thermal imagery; we can estimate the GeoGauge stiffness for all soils but the Stability pit. Between these two different soil strength measurements, we are able to predict all five soil type strengths, whether that is in terms of cone index (psi) or stiffness (Mega-Netwon/meter). The ATI to mean soil strength values have R^2 values for of 0.9281 for GeoGauge stiffness and 0.8372 for cone penetrometer. Linear regression was built based on field collection to develop prediction plots.

Initial results are promising from both the field and the laboratory data, indicating that utilizing both thermal and hyperspectral imaging, we can derive useful inputs such as soil gradation, cone index, and soil stiffness for terrain strength characterization. Hence through remote sensing, a less expensive, more rapid, and safer method of data collection for soldiers to gather soil strength can be utilized for mobility modeling and simulation.

5. CONCLUSIONS AND FUTURE WORK

In conclusion, using hyperspectral imagery, we were able to build soil gradation prediction plots utilizing only remotely collected data. This method is possible using SCI and its ability to predict the gradation of the soil: % gravel, % sand, and % fine content. These predicted soil gradations could help give us the estimates of soil type for the soil pits we tested.

The use of thermal imagery provides a method for collecting the ATI of each soil pit. The ATI is correlated to both the in-situ measurements of GeoGauge stiffness and cone penetrometer measurements. These in-situ measurements are an estimate of the soil strength at a particular location. This soil strength can, therefore, now be predicted using only remotely collected values. Hence, we

are able to now develop soil strength maps remotely, without the necessity of in-situ measurements.

With the combinations from both sensors, one can develop the best approximation for the soil strength remotely, and thereby allow a safer methodology for Go/No Go mobility map development. In the future, we hope to utilize machine learning to help enhance this prediction. With the use of machine learning, we also hope to look at other band combinations to help derive potentially more indices like the SCI, that could identify more features within the soil. Through the use of these new indices or by using more or all available hyperspectral bands, we hope to identify relationships to other key soil properties, which could allow for a full USCS classification scheme. We also hope to examine more soil types this summer in the Upper Peninsula over a larger area. This next study will also include more in-situ strength measurements and on-site moisture content readings at several site locations with variable soil types for robust validation and uncertainty quantification. Our study site will overlap with the NASA G-LiHT (Goddard's LiDAR, Hyperspectral & Thermal Imager) manned aircraft to allow for a comparison across different platforms for scalability.

6. ACKNOWLEDGMENTS

We would like to thank the University of Michigan's Automotive Research Center (ARC), the U.S. Army Combat Capabilities Development Command Ground Vehicle Systems Center (CCDC - GVSC, formerly TARDEC), and Michigan Technological University (MTU) for funding this research. We would also like to thank the Keweenaw Research Center (KRC) for providing the logistics for data collection.

1. REFERENCES

[1] J. A. Okello, "A Review of Soil Strength Measurement Techniques for Prediction of Terrain Vehicle Performance," Journal of agricultural engineering research, vol. 50, pp. 129-155, 1991. [Online]. Available: https://doi.org/10.1016/S0021-8634(05)80010-1.

[2] S. A. Shoop, "Terrain Characterization for Trafficability," US Army Corps of Engineers Cold Regions Research & Engineering Laboratory, CRREL Report 93-6, 1993.

[3] D. M. McCullough, D. P. Jayakumar, D. J. Dasch, and D. D. Gorsich, "Developing the Next Generation NATO Reference Mobility Model," Proceedings of the 2016 Ground Vehicle Systems Engineering and Technology Symposium (GVSETS), 2016.

[4] Standard Practice for Classification of Soils for Engineering Purposes (Unified Soil Classification System), ASTM, 2019.

[5] S. Cola and P. Simonini, "Mechanical behavior of silty soils of the Venice lagoon as a function of their grading characteristics," Canadian Geotechnical Journal, vol. 39, no. 4, pp. 879-893, 2002, doi: 10.1139/t02-037.

[6] B. Minasny and A. B. McBratney, "Digital soil mapping: A brief history and some lessons," Geoderma, vol. 264, pp. 301-311, 2016, doi: 10.1016/j.geoderma.2015.07.017.

[7] N. Stark, J. McNinch, H. Wadman, H. C. Graber, A. Albatal, and P. A. Mallas, "Friction angles at sandy beaches from remote imagery," Géotechnique Letters, vol. 7, no. 4, pp. 292-297, 2017, doi: 10.1680/jgele.17.00053.

[8] G. A. Shaw and H.-h. K. Burke, "Spectral Imaging for Remote Sensing," LINCOLN LABORATORY JOURNAL, vol. 14, no. 1, 2003.

[9] D. Sousa and C. Small, "Multisensor Analysis of Spectral Dimensionality and Soil Diversity in the Great Central Valley of California," Sensors (Basel), vol. 18, no. 2, Feb 14 2018, doi: 10.3390/s18020583.

[10] M. Vohland, M. Ludwig, S. Thiele-Bruhn, and B. Ludwig, "Quantification of Soil

Properties with Hyperspectral Data: Selecting Spectral Variables with Different Methods to Improve Accuracies and Analyze Prediction Mechanisms," Remote Sensing, vol. 9, no. 11, 2017, doi: 10.3390/rs9111103.

[11] M. Strojnik, P. Merola, A. Allegrini, D. Guglietta, and S. Sampieri, "Buried archaeological structures detection using MIVIS hyperspectral airborne data," presented at the Infrared Spaceborne Remote Sensing XIV, 2006.

[12] S. S. Bishop et al., "Airborne thermal infrared hyperspectral imaging of buried objects," presented at the Detection and Sensing of Mines, Explosive Objects, and Obscured Targets XX, 2015.

[13] B. Zwissler, T. Oommen, S. Vitton, and E. A. Seagren, "Thermal Remote Sensing For Moisture Content Monitoring of Mine Tailings: Laboratory Study," Environmental and Engineering Geoscience, vol. 23, no. 4, pp. 299-312, 2017, doi: 10.2113/gseegeosci.23.4.299.

[14] K. V. S. Badarinath and T. R. K. Chand, "ANALYSIS OF APPARENT THERMAL INERTIA OVER DIFFERENT LAND USE / LAND COVER TYPES USING ENVISAT AATSR DATA," Journal of the Indian Society of Remote Sensing, vol. 35, no. 2, 2007.

[15] R. González, A. López, and K. Iagnemma, "Thermal vision, moisture content, and vegetation in the context of off-road mobile robots," Journal of Terramechanics, vol. 70, pp. 35-48, 2017, doi: 10.1016/j.jterra.2017.01.001.

[16] J. L. B. Philip R. Christensen, James F. Bell III, Noel Gorelick, Victoria E. Hamilton,, B. M. J. Anton Ivanov, Hugh H. Kieffer, Melissa D. Lane,, T. M. Michael C. Malin, Alfred S. McEwen, Harry Y. McSween Jr.,, J. E. M. Greg L. Mehall, Kenneth H. Nealson, James W. Rice Jr., MarkI. Richardson,, and M. D. S. Steven W. Ruff, Timothy N. Titus, Michael B. Wyatt, "Morphology and Composition of the Surface of Mars: Mars Odyssey THEMIS Results," Science, pp. 2056-2061, 2003.

[17] N. Putzig and M. Mellon, "Apparent thermal inertia and the surface heterogeneity of Mars," Icarus, vol. 191, no. 1, pp. 68-94, 2007, doi: 10.1016/j.icarus.2007.05.013.

[18] B. C. Sahoo, T. Oommen, D. Misra, and G. Newby, "Using the one-dimensional S-transform as a discrimination tool in classification of hyperspectral images," Canadian Journal Remote Sensing, vol. 33, no. 6, pp. 551-560, 2007.

[19] T. Oommen, L. G. Baise, R. Gens, A. Prakash, and R. P. Gupta, "Documenting Earthquake-Induced Liquefaction Using Satellite Remote Sensing Image Transformations," Environmental & Engineering Geoscience, vol. 19, no. 4, pp. 303-318, 2013, doi: 10.2113/gseegeosci.19.4.303.

[20] E. H. Bouali, T. Oommen, S. Vitton, and R. Escobar-Wolf, "Rockfall Hazard Rating System: Benefits of Utilizing Remote Sensing," Environmental & Engineering Geoscience, vol. 23, no. 3, pp. 165–177, 2017.

[21] J. R. Jensen, "Remote sensing of the environment: An earth resource perspective 2/e," 2009.

[22] M. Minacapilli, Cammalleri, C., Ciraolo, G., D'Asaro, F., Iovino, M., and Maltese, A., "Thermal Inertia Modeling for Soil Surface Water Content Estimation: A Laboratory Experiment," Soil Science Society of America Journal, vol. 76, no. 1, pp. 92-100, 2012, doi: 10.2136/sssaj.